

**Influence of disordered porous media on the anomalous properties of a simple water model**A. P. Furlan,<sup>1,\*</sup> Carlos E. Fiore,<sup>2,†</sup> and M. C. Barbosa<sup>1,‡</sup><sup>1</sup>*Instituto de Física, Universidade Federal do Rio Grande do Sul, Caixa Postal 15051, 91501-570, Porto Alegre, RS, Brazil*<sup>2</sup>*Instituto de Física, Universidade de São Paulo, Caixa Postal 19044, 81531 São Paulo, SP, Brazil*

(Received 17 April 2015; published 15 September 2015)

The thermodynamic, dynamic, and structural behavior of a water-like system confined in a matrix is analyzed for increasing confining geometries. The liquid is modeled by a two-dimensional associating lattice gas model that exhibits density and diffusion anomalies, similar to the anomalies present in liquid water. The matrix is a triangular lattice in which fixed obstacles impose restrictions to the occupation of the particles. We show that obstacles shorten all lines, including the phase coexistence, the critical and the anomalous lines. The inclusion of a very dense matrix not only suppresses the anomalies but also the liquid-liquid critical point.

DOI: [10.1103/PhysRevE.92.032404](https://doi.org/10.1103/PhysRevE.92.032404)

PACS number(s): 68.08.–p, 61.20.Gy, 61.20.Ja

**I. INTRODUCTION**

The phase behavior of systems of particles interacting via the so-called core-softened (CS) potentials has received a lot of attention recently. They show a repulsive core with a softening region when particles are very close and an attractive region when particles are more distant. These CS can be modeled as continuous potentials or lattice gas models. For the lattice structure the two competing scales arise from two equilibrium configurations: low density and high density. This procedure generates models that are analytically and computationally tractable and that one hopes are capable of retaining the qualitative features of the real complex systems. The physical motivation behind these studies is the assumption that two length scales systems exhibit the same anomalous behaviors present in water. Confirming this hypothesis a number of continuous [1–7] and lattice gas models [8–16] show the presence of density, diffusion, and structural anomalous behavior as observed in water [17,18].

Within the other 72 anomalies [19], water has at very low temperatures two coexisting amorphous phases with distinct densities: the low-density amorphous (LDA) and high-density amorphous phases (HDA) [20–24]. These two amorphous phases led to the hypothesis of the existence at higher temperatures of two liquid phases: a low-density liquid and high-density liquid phases. Such conjecture establishes that the coexistence between these two liquid phases ends in a second critical point or also called, liquid-liquid critical point (LLCP) [24]. Experiments for testing the existence of this criticality are difficult since the region in the pressure versus temperature phase diagram where the alleged critical point exists is located beyond the homogeneous nucleation limit. In order to circumvent this difficulty for testing the existence of the liquid-liquid critical point, recently confined geometries have been employed [25,26]. In these nanoconfined geometries the disruption of the hydrogen bonds suppresses the solidification of the system and allows for maintaining the system liquid in temperatures in which otherwise would be solid [25,26]. These experimental systems show convincing evidences that water exhibits two liquid structures at low temperatures.

The use of water confined, however, brings another set of issues. What guarantees that the same thermodynamic and dynamic anomalies and criticality present in the unconfined system are not destroyed as the system is confined? Can confinement bring up new phenomena not present in the unconfined geometries? In order to answer these questions water-like atomistic or continuous effective potential models were explored. The confining geometries could be plates [27–37], one pore [38–46], and a disordered matrix [43,52,53,55–57]. The results for the melting temperature obtained within these approaches are controversial, while results for SPC/E water show that the melting temperature for hydrophobic plates is lower than the melting for the unconfined system and higher than for the system confined by hydrophilic walls, for the mW model no difference between the melting temperatures due to the hydrophobicity [47] is found.

Other quantities, such as the TMD and the diffusion extrema show a definitive trend. In confined systems the TMD occurs at lower temperatures for the hydrophobic confinement [48,49] and at higher temperatures for the hydrophilic confinement [50] when compared with the unconfined system. The diffusion coefficient,  $D$ , in the direction parallel to the plates exhibits the same anomalous behavior observed in unconfined water. However, the temperatures of the maximum and minimum of  $D$  are lower for the confined system when compared with the unconfined water [49]. In the direction perpendicular to the plates, no diffusion anomalous behavior is observed [51].

In addition to the usual density and diffusion anomalous behavior, these confined systems show a variety of new effects not present in the unconfined system. For example, fluids confined in carbon nanotube exhibit formation of layers, crystallization of the contact layer [58,59], and a superflow not present in macroscopic confinement [60,61]. The confinement by a pore, within plates or nanotubes, is symmetric, and even though it introduces a breaking of the water-hydrogen bond network, this is done in an ordered way. Confining matrix such as the ones present in plants and underground water are not ordered. The idea of exploring the random confinement is quite appealing and have generated some discussion in the literature [62,63]. For instance, recently the effects of a water-like liquid confined in a disordered matrix have been analyzed using a model in which the bonds are introduced by the inclusion of Potts variables [53,54]. This study shows that the liquid-liquid coexistence line is affected by the increase of the density of random porous in the matrix.

\*furlan@if.ufrgs.br

†fiore@if.usp.br

‡marcia.barbosa@ufrgs.br

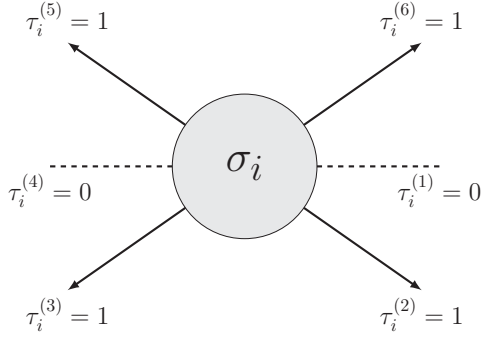


FIG. 1. The occupational and orientational states of a molecule at the site  $i$ . The arms variables are:  $\tau_i^{(1)} = 0$ ,  $\tau_i^{(2)} = 1$ ,  $\tau_i^{(3)} = 1$ ,  $\tau_i^{(4)} = 0$ ,  $\tau_i^{(5)} = 1$ ,  $\tau_i^{(6)} = 1$ .

In all these studies, however, the liquid-liquid transition is preserved and the density of confining matrix is not very high. Here, we give a further step by investigating effects imposed by disordered porous when the random matrix exhibits a high density. The system is defined in a triangular lattice where the obstacles are fixed and randomly distributed. The fluid is modeled as the associating lattice gas (ALG) model [12] defined in terms of an occupational variable together with a bond orientational variable. This model shows the density and diffusion anomalies present in real water and also exhibits the liquid-gas and liquid-liquid phase coexistence [12]. Here we explore the effects in the chemical potential versus temperature phase diagram of the presence of the random fixed obstacles in an attempt to mimic the natural random structures.

This paper is organized as follows. In Sec. II we present the model used here. In Sec. III we outline details of Monte Carlo (MC) simulations and how the thermodynamic properties of system were calculated. Results are presented in Sec. IV, followed by conclusions in Sec. V.

## II. THE MODEL

The ALG model is defined in a triangular lattice, in which each accessible site  $i$  can be empty or occupied by a water molecule. Empty sites have  $\sigma_i = 0$ , while occupied sites have  $\sigma_i = 1$ . Each water molecule has orientational states represented by the variable  $\tau$  that presents six arms, two being inert arms with  $\tau_i = 0$  and four being active arms with  $\tau_i = 1$ . They represent the possibility of a molecule to form hydrogen bonds with up to four neighbor molecules. The two inert arms are diametrically positioned, in such a way that there are just three different orientational states. Figure 1 exemplifies the geometry of the model.

A bond is formed only when the active arms of two neighbor molecules point out to each other, namely  $\tau_i \tau_j = 1$ . In this case, the interaction energy between two bonded arms reads  $-v$  while nonbonded arms contribute with a higher energy of  $-v + 2u$  (punishment for nonforming hydrogen bonds). The Hamiltonian of the system is given by

$$\mathcal{H} = 2u \sum_{(i,j)} \sigma_i \sigma_j \left[ \left(1 - \frac{v}{2u}\right) - \tau_i \tau_j \right] - \mu \sum_i \sigma_i. \quad (1)$$

The phase behavior of the system in the absence of obstacles was already analyzed in a previous publication [15] and it

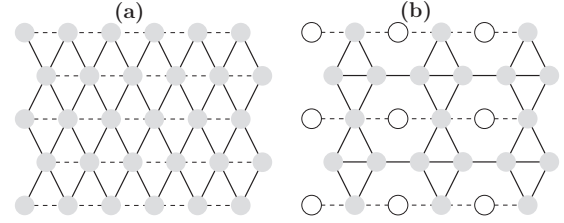


FIG. 2. Examples of a configuration for the HDL (a) and LDL (b) phases for the associating lattice gas (ALG) model. The solid and dashed lines indicate the bonding and inert arms, respectively.

is reviewed as follows. At ground state,  $T^* \equiv T/v = 0$ , the grand potential per site is  $\Phi = e - \mu N$  where  $e = \langle \mathcal{H} \rangle / L^2$ . At low chemical potentials, the lattice is empty and the system is constrained in gas phase,  $\rho = 0$ . In this phase the grand potential is  $\Phi_G = 0$ . Increasing the chemical potential the system reaches a point at which the gas phase coexists with a low-density liquid phase (LDL). In this phase, the density is  $\rho = 3/4$  and each particle forms four hydrogen bonds with its neighbors, resulting in a grand potential per site  $\Phi_{\text{LDL}}/L^2 = -(3/2)v - (3/4)\mu$  and consequently in a gas-LDL coexistence chemical potential  $\mu_{\text{G-LDL}}^* = \mu_{\text{G-LDL}}/v = -2$ . For high chemical potentials, all sites of lattice are occupied by particles, resulting in a density  $\rho = 1$  and grand potential per site  $\Phi_{\text{HDL}}/L^2 = -3v + 2u - \mu$ . The coexistence between the LDL phase and the HDL phase occurs at  $\mu_{\text{LDL-HDL}}^* = \mu_{\text{LDL-HDL}}/v = 8u/v - 6$ . The main features of LDL and HDL phases are exemplified in Fig. 2 for two possible configurations at  $T^* = 0$ .

At temperatures  $T^* \equiv T/k_B v > 0$ , the model was also already analyzed by Monte Carlo simulations [15]. The chemical potential versus temperature phase diagram is shown in the Fig. 3(a).

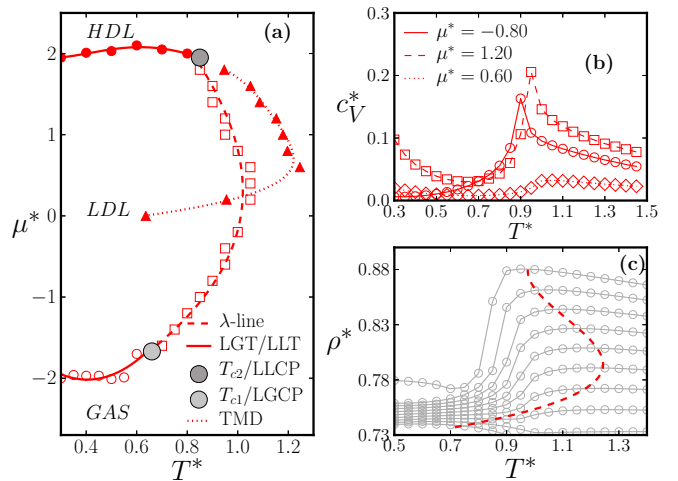


FIG. 3. (Color online) For the ALG model, panel (a) shows the phase diagram  $\mu^*$  vs.  $T^*$ , illustrating the gas-LDL (empty circles) and the LDL-HDL (filled circles) phase transitions, the  $\lambda$ -line (empty squares), and the TMD line (filled triangles). In panel (b) we plot the  $c_V^*$  vs.  $T^*$  for  $\mu^* = -0.80$  (circles),  $\mu^* = 0.60$  (diamonds), and  $\mu^* = 1.20$  (squares). In (c) the system density  $\rho$  vs.  $T^*$  for fixed  $\mu^*$  along the TMD line (dashed line).

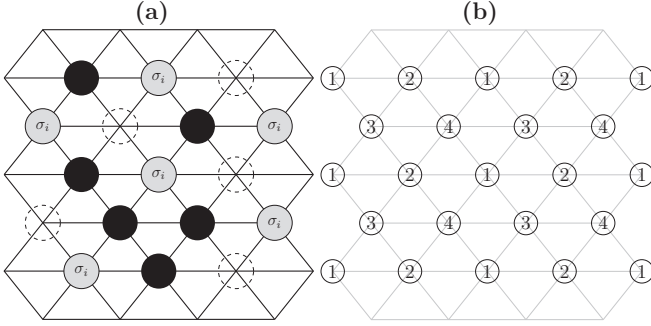


FIG. 4. Left panel shows a lattice configuration where the solid gray, the solid black, and the dashed circles describe water molecules, obstacles, and empty sites, respectively. For clarity, the bonds are not shown. Right panel shows a lattice configuration with the subdivision in four sublattices.

The gas-LDL and LDL-HDL transition lines are first-order transitions, ending in the tricritical points  $T_{c1}^*$  and  $T_{c2}^*$ , respectively. These two tricritical points are connected by a line of continuous transitions, the  $\lambda$  line. For the ALG model with no obstacles the tricritical temperatures,  $T_{c1}^* = 0.65$  and  $T_{c2}^* = 0.825$ , respectively. In order to understand the differences between the LDL and HDL phases, the lattice as shown in the Fig. 4(a) is divided in four sublattices as illustrated in the Fig. 4(b). The LDL phase is characterized by one of the sublattices being empty while all the others are filled, in such a way that the transition to the HDL phase occurs when the empty sublattice is filled. Also, it is signed by a rotation in the inert arms, in which in the HDL phase they are all parallel. In the LDL phase, each particle forms four bonded arms that show a zigzag structure, whereas in the HDL phase each particle also forms four bonded arms but with parallel lines.

The density of bonds,  $\rho_{hb} = \frac{1}{L^2} \sum_{i=1}^{L^2} \sum_{i+\delta} \sigma_i \sigma_{i+\delta} \tau_i \tau_{i+\delta}$  is also an important quantity for characterizing the phase transitions. At  $T^* = 0$  the gas, LDL, and HDL phases has  $\rho_{hb}$  reading 0, 1.5, and 2, respectively. Thus the phase transitions are also signed by changes in the fraction of hydrogen bonds. At very high temperature the system is disordered. The sublattice occupations do not exhibit any ordering. By lowering  $T^*$ , the  $\lambda$  line is crossed, which one sublattice is emptied and the others remaining filled with an reorganization of the inert arms that form the above ordered zig-zag structure. This the  $\lambda$  line transition is identified by the peak of the specific heat at constant volume  $c_V$  [15].

In this work the disordered porous media is introduced by considering fixed obstacles that are randomly distributed in the lattice. Each obstacle occupies a single site and interacts with the particles via a “hard-core” constraint. The density of obstacles is given by  $\rho_o = N_o/L^2$ , where  $N_o$  is the number of obstacles and  $L^2$  is the system volume. In Fig. 4(a), a lattice configuration composed of water, obstacles, and empty sites is exemplified.

### III. THE METHODS AND SIMULATION DETAILS

Numerical simulations have been performed for the triangular lattices of size  $L = 35$  and periodic boundary conditions.

Three representative values for the density of obstacles  $\rho_o = 0.08, 0.24,$  and  $0.40$  have been considered.

In all cases, we have used  $10^6$  MC steps to equilibrate the system and  $10^6$  MC steps for evaluating the relevant quantities. Each Monte Carlo step is defined as the number of  $L^2$  trials for generating new configurations, including the choice of empty sites and water molecules. Additional simulations for  $L = 24, 35, 40, 56,$  and  $80$  and finite-size scaling analysis were performed in order to study the critical lines and to test size effects in the porosity.

All the thermodynamic properties have been obtained by performing grand canonical MC simulations for fixed  $T^*, \mu^* \equiv \mu/v,$  and  $\rho_0$  [64]. Microscopic configurations are generated according to the Metropolis algorithm [65] described as follows. First, the obstacles are randomly distributed. Then, a site  $k$  not occupied by an obstacle is randomly selected. If the site  $k$  is not occupied, an attempt to occupy the site with a water molecule in a randomly selected arm orientation is made. If the site  $k$  is already occupied by a water molecule one of the following actions are tried: to empty the site or to change the arm configuration of the water molecule to one of the other two possible states. Next, to accept or not the attempts to change the site occupation, the energy difference  $\Delta\mathcal{H}$  between the original and the new configuration is computed. The configuration change is accepted according to the Metropolis prescription  $\min\{1, e^{-\beta\Delta\mathcal{H}}\}$ , where  $\beta = 1/k_B T$ . As mentioned previously, this process is first repeated  $10^6$  times without computing and after this, thermodynamic quantities are averaged over  $10^6$  Monte Carlo steps.

Some remarks over the obstacles distributions are required. In principle, a random distribution might lead to statistical problems. According to some works [66,67], systems with random disorder lose the self-averaging, and averages over many distributions of obstacles are required. However, this affects mainly the computation of critical temperatures and exponents. In the present case, by performing tests with different random distributions of obstacles, we have verified that the tested temperatures and chemical potentials led to results not sensitive to the specific distribution of obstacles. Then, for simplicity only one random distribution was employed. For calculating the critical  $\lambda$  line, we considered the peak of the specific heat at constant volume, given by

$$c_V = \frac{1}{VT^2} \left[ \langle \delta\mathcal{H}^2 \rangle_{\text{gcan}} - \frac{\langle \delta\mathcal{H}\delta N \rangle_{\text{gcan}}^2}{\langle \delta N^2 \rangle_{\text{gcan}}} \right] + \frac{3Nk_B}{2V}, \quad (2)$$

where  $\delta X = X - \langle X \rangle$  with  $X = \mathcal{H}$  and  $N$  and averages are evaluated in the ensemble of  $T, \mu$  fixed. The chemical potentials and temperatures of the  $\lambda$  line were obtained through the finite-size scaling analysis of  $c_V$  employing  $L = 24, 35, 40, 56,$  and  $80$ .

In addition to the thermodynamic quantities, the influence of obstacles in the dynamic properties was also investigated. Since we perform Monte Carlo simulations, the dynamics is characterized through the diffusion coefficient  $D$  given by Einstein’s relation

$$D = \lim_{t \rightarrow \infty} \frac{\langle \Delta r(t)^2 \rangle}{4t}, \quad (3)$$

where  $\langle \Delta r(t)^2 \rangle = \langle [r(t) - r(0)]^2 \rangle$  is the mean-square displacement per particle and time is measured in Monte Carlo steps. Although the diffusion coefficient (measured under Monte Carlo simulations) is a stochastic dynamics and not a real space mobility, it is possible to associate the former with the concept of diffusion anomalous like the behavior observed in liquid water [16]. The numerical MC procedure for calculating the diffusion is described as follows. First, the system is equilibrated by employing the previous Metropolis dynamics for fixed  $T^*$  and  $\mu^*$ . After the equilibrium is reached, an occupied site  $i$  and its neighbor  $j$  are chosen randomly. If neighbor site  $j$  is empty, the molecule moves to the empty site also following the above Metropolis prescription  $\min\{1, e^{-\beta\Delta\mathcal{H}}\}$ , where  $\Delta\mathcal{H}$  is the difference of energy due to the movement. A Monte Carlo step  $t$  is defined through the number of trials of movement for all system particles. After repeating this algorithm  $nt$  times, where  $n$  is the number of molecules in the lattice, the diffusion coefficient is calculated from Eq. (3). Here we employ  $t = 800$  for the evaluations.

#### IV. RESULTS

##### A. Structural and thermodynamic behavior

First, let us examine what happens with the phases present in the system as the obstacles are introduced. Figure 5 shows the water density  $\rho$ , versus the reduced chemical potential  $\mu^*$ , for distinct porous densities at the fixed temperature  $T^* = 0.40$ . Figure 5 also shows that for  $T^* = 0.40$  the gas-LDL

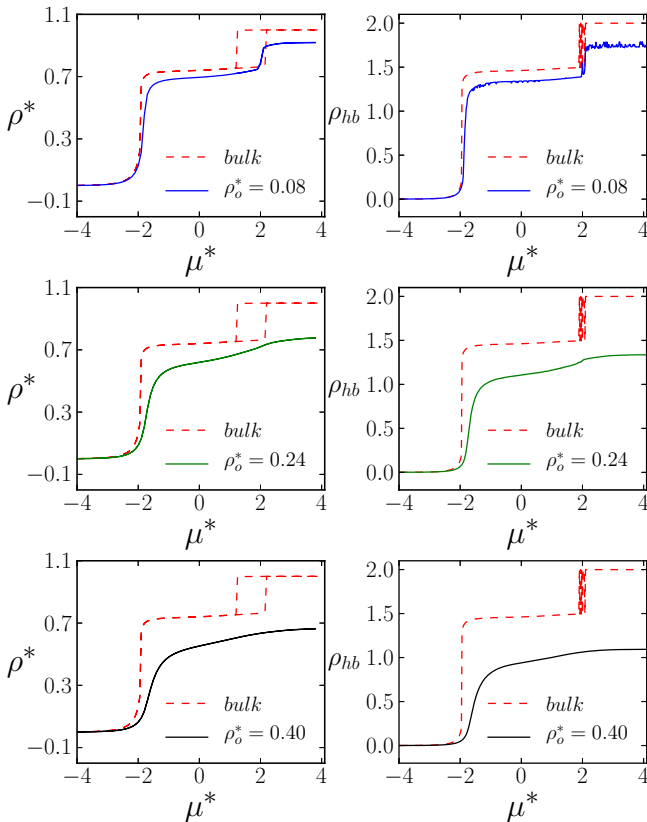


FIG. 5. (Color online)  $\rho$  vs.  $\mu^*$  for distinct porous densities  $\rho_o$  for  $T^* = 0.40$ .

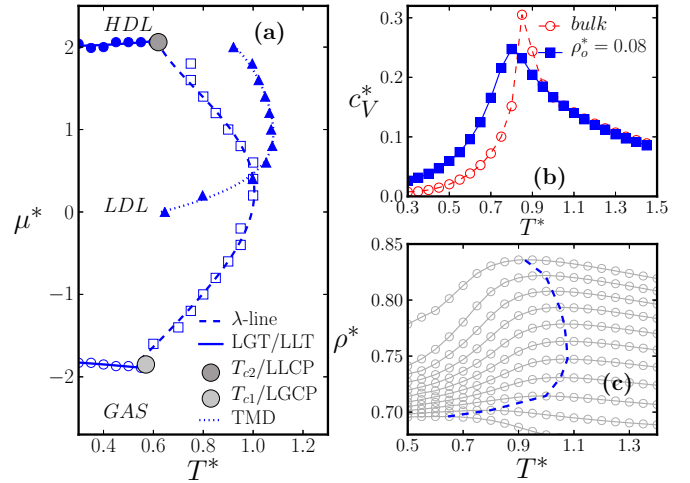


FIG. 6. (Color online) For  $\rho_o = 0.08$ : (a) Chemical potential  $\mu^*$  vs. reduced temperature  $T^*$  phase diagram showing the Gas-LDL (empty circles), the LDL-HDL (filled circles) phase transitions, the  $\lambda$ -line (empty squares), and the TMD line (filled triangles). (b) Specific heat at constant volume  $c_V$  vs.  $T^*$  for the system with obstacles (filled squares) and system with no obstacles (empty circles) at  $\mu^* = -1.00$ . Panel (c)  $\rho$  versus  $T^*$  for  $\mu^* = 0.0, \dots, 2.2$  showing the TMD line (dashed line).

phase exhibits a smaller hysteresis loop when compared with the LDL-HDL transition. This indicates that the gas-LDL free-energy barrier is smaller than the LDL-HDL barrier. This also reflects in the difference between the gas-LDL tricritical temperature,  $T_{c1}^*$ , which is smaller than the LDL-HDL tricritical temperature,  $T_{c2}^*$ . The size of the hysteresis loops change with the temperature and lattice size but in all the analyzed cases the gas-LDL is much smaller than the LDL-HDL loop.

The inclusion of obstacles changes the temperature and chemical potential locations of the gas-LDL and the LDL-HDL phase transition. In particular, the increase in the number of obstacles leads to the disruption of the hydrogen bonds, decreasing the free-energy barriers separating the coexisting phases. This explains the decrease in the hysteresis loop when obstacles are included. In addition, the density gap between the two liquid phases becomes less abrupt and the inclusion of obstacles moves the transition points to larger chemical potentials.

Figures 6, 7, and 8 illustrate the chemical potential versus temperature phase diagrams for  $\rho_o = 0.08, 0.24$ , and  $0.40$ , respectively. In particular, by increasing  $\rho_o$  the tricritical points  $T_{c1}^*$  and  $T_{c2}^*$ , in which the gas-LDL and LDL-HDL coexistence lines meet the  $\lambda$  line, decrease as shown in Figs. 6, 7, and 8. More specifically, while for the system without obstacles the gas-LDL tricritical point is located at  $T_{c1} = 0.65$ , it moves to  $T_{c1}^* = 0.60, 0.55$ , and  $0.52$  for  $\rho_o = 0.08, 0.24$ , and  $0.40$ , respectively.

This scenario becomes even more drastic in the case of the LDL-HDL phase transition. The tricritical point not only decreases its value from  $T_{c2}^* = 0.825$  (no obstacles) to  $T_{c2} = 0.57$  and  $T_{c2} = 0.52$  for  $\rho_o = 0.08$  and  $0.24$ , respectively, but the critical line disappears for  $\rho_o = 0.40$ , implying the absence of liquid-liquid transition line.

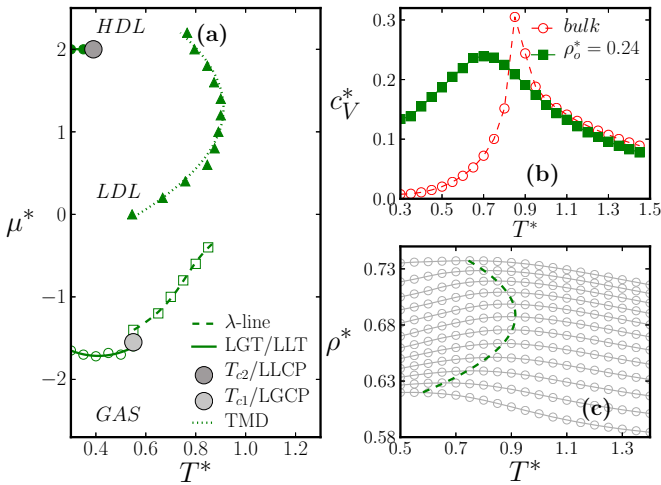


FIG. 7. (Color online) For  $\rho_o = 0.24$ : (a) Chemical potential  $\mu^*$  vs. reduced temperature  $T^*$  phase diagram showing the Gas-LDL (empty circles), the LDL-HDL (filled circles) phase transitions, the  $\lambda$ -line (empty squares), and the TMD line (filled triangles). (b) Specific heat at constant volume  $c_V$  vs.  $T^*$  for the system with obstacles (filled squares) and system with no obstacles (empty circles) at  $\mu^* = -1.00$ . Panel (c)  $\rho$  versus  $T^*$  for  $\mu^* = 0.0, \dots, 2.0$  showing the TMD line (dashed line).

The changes in the transition points can be understood by verifying that the inclusion of obstacles suppress partially the structured patterns found in the LDL and HDL phases (see, e.g., Figs. 2(a) and 2(b) for the zero obstacle system). In the case of the LDL phase the ordered structure is distorted as  $\rho_o$  increases, as illustrated in Fig. 9 for  $\mu^* = -0.5$ . For the lowest case  $\rho_o = 0.08$ , the degree of confinement is low and most occupied sites preserve at least three bonds. As  $\rho_o$  is

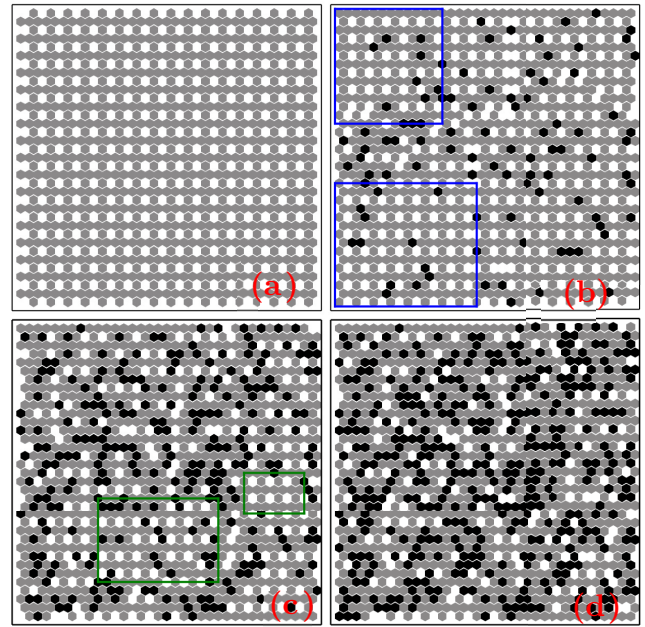


FIG. 9. (Color online) Spatial snapshot ( $35 \times 35$  sites) of triangular lattice. Each site is represented by hexagon, with its six nearest-neighbor sites. White hexagons represent vacancies, black represent obstacles, and gray represent water-like particles. The snapshots exhibit character configurations of system with chemical potential  $\mu^* = -0.5$  and temperature  $T^* = 0.3$ . In (a) we present the unconfined system. In (b) the system submitted at low degree of confinement  $\rho_o = 0.08$  and the blue rectangles denote the regions where the characteristic geometry of LDL of ALG is preserved. In (c), intermediate degree of confinement  $\rho = 0.24$ , and green rectangles denote the LDL structure. The highest degree of confinement  $\rho = 0.40$  is shown in (d).

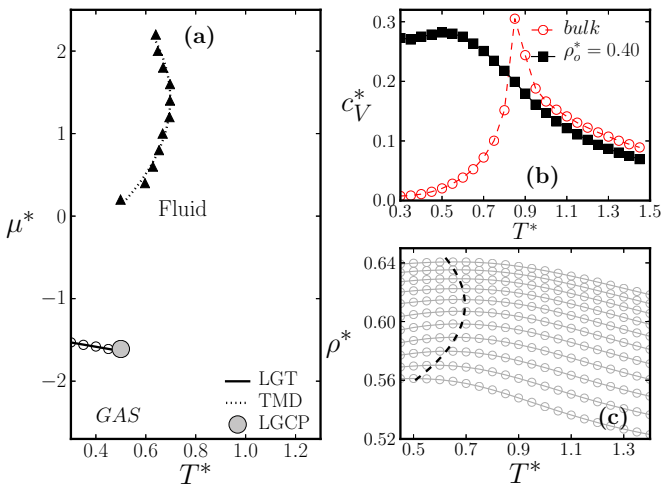


FIG. 8. (Color online) For  $\rho_o = 0.40$ : (a) Chemical potential  $\mu^*$  vs. reduced temperature  $T^*$  phase diagram showing the Gas-LDL (empty circles), the LDL-HDL (filled circles) phase transitions, the  $\lambda$ -line (empty squares), and the TMD line (filled triangles). (b) Specific heat at constant volume  $c_V$  vs.  $T^*$  for the system with obstacles (filled squares) and system with no obstacles (empty circles) at  $\mu^* = -1.00$ . Panel (c)  $\rho$  versus  $T^*$  for  $\mu^* = 0.0, \dots, 2.0$  showing the TMD line (dashed line).

raised (here exemplified for  $\rho_o = 0.24$  and  $0.40$ ) the fraction of disrupted bonds increases, reaching a limit in which the connectivity of the network is lost. Similar effect is verified in the HDL phase, but the effect is more pronounced in such case. This can be understood by recalling that in the LDL phase, obstacles occupy partially empty sites with neighboring molecules not forming hydrogen bonds. Thus, the disruption of hydrogen bonds is more relevant in the HDL phase.

This loss of connectivity also explains why the transition from the disordered structure to the LDL through the  $\lambda$  line occurs for lower temperatures when compared with the temperatures obtained for the system with no obstacles. For example, for  $1 - \mu^* = -1$  and distinct obstacle densities  $\rho_o = 0.08$  and  $\rho_o = 0.24$ , analysis of the peak of  $c_V^*$  show (in all cases) a scaling with  $L^{-1}$ , from which we obtain the critical temperatures  $T_c^* = 0.795(1)$  and  $0.717(1)$ , respectively. These estimates are lower than  $0.866(1)$ , obtained for the unconfined system. This transition is an order-disorder transition in which one of the sublattices becomes empty while the others are filled; consequently, the increase of number of obstacles increases the entropy by breaking bonds that favor a disordered phase.

Thus, all transition points move for lower temperatures as a way for “compensating” the above increase of disorder. In other words, due to the inclusion of obstacles, the structured phases exist only for lower temperatures than in the unconfined

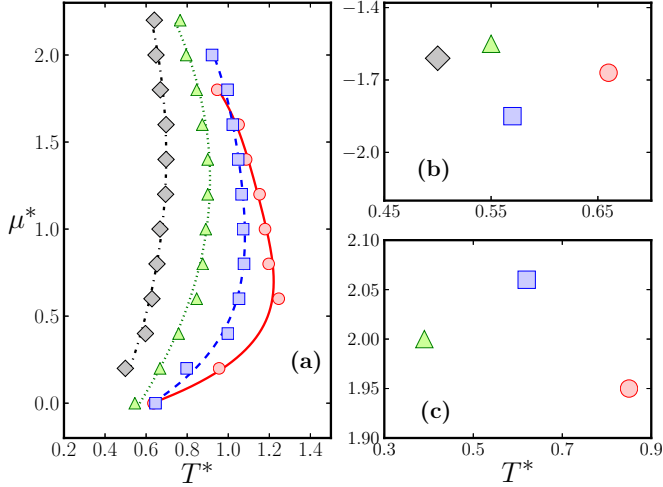


FIG. 10. (Color online) Chemical potential versus temperature illustrating (a) the TMD lines, (b) the gas-LDL tricritical point, and (c) the LDL-HDL critical point values for the unconfined (circles) and the system with different concentrations of obstacles. The squares, triangles, and diamonds correspond to  $\rho_o = 0.08, 0.24,$  and  $0.40,$  respectively.

system, whose decreasing become more pronounced as  $\rho_o$  increases. Finally, for high density of obstacles the  $\lambda$ -line transition is destroyed by fluctuations. The last comment concerns the comparison between the TMD as  $\rho_o$  increases, as shown in Fig. 10. As for the transition lines, the TMD shortens and move for lower temperatures (with maximum  $\rho$  decreasing) as  $\rho_o$  increases. However, in contrast with previous results, for  $\rho_o = 0.40$  a tiny TMD (ranged from  $T^* = 0.50$  to  $0.70$  with  $\rho = 0.56$  to  $0.64$ ) is verified.

### B. Diffusion and dynamic anomaly

Besides the influence of the immobile obstacles in the thermodynamic quantities, another relevant question concerns what happens with the water mobility as the density of obstacles increases.

Figure 11 shows the diffusion coefficient computed using Eq. (3) for different  $T^*$ 's and  $\rho_o$ 's. Similar to what happens for the ALG model with no obstacles, the diffusion coefficient presents a region in densities in which  $D$  increases with  $\rho$ . This is the so-called diffusion anomaly also present in water. The addition of obstacles shrinks the region in temperatures and pressures in which the diffusion anomaly is present and for  $\rho_o = 0.40$  no diffusion anomaly is observed.

The dynamic anomaly depends crucially on the presence of a high number of neighbor sites occupied by the fluid [68]. The obstacles make this difficult, and for a very high number of obstacles, the mobility becomes even impossible.

Since for water-like systems, typically the region in the  $\mu^*$ - $T^*$  phase diagram in which the density anomaly is present is close to the region where the diffusion anomaly appears.

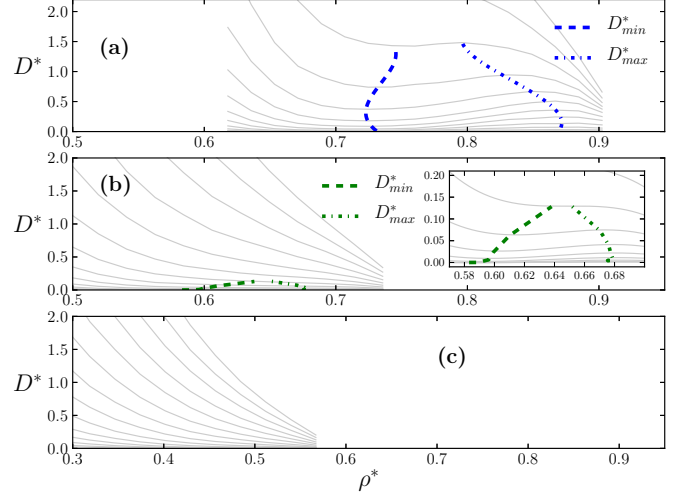


FIG. 11. (Color online) Diffusion coefficient versus density at fixed temperatures for: (a)  $\rho_o = 0.08,$  (b)  $\rho_o = 0.24,$  and (c)  $\rho_o = 0.40.$  The solid gray lines are the values of the diffusion coefficient for  $T^* = 0.30 \dots 1.00$  with  $\Delta T^* = 0.05$  (from bottom to top), the blue dashed and dot-dashed lines connect the minimum and maximum in  $D,$  respectively.

Therefore, one expects that the suppression of the first is directly related to the disappearance of the other.

## V. CONCLUSION

The effects of fixed obstacles in thermodynamic and dynamic properties of a simplified water-like model have been investigated. For low degree of confinement, the thermodynamic, structural, and dynamic properties of model are almost totally preserved due to the low steric effects. For the intermediate case,  $\rho_o = 0.24,$  the system suffers significant changes, such as the decrease of the critical and tricritical points to lower temperatures, resulting in a reduction of coexistence regions. This effect is more dramatic for the liquid-liquid coexistence that disappear for  $\rho_o = 0.40.$  The density and diffusion anomalous regions are also shifted to lower temperature, keeping the reduction in temperature-chemical potential phase diagram. The disappearance of the liquid-liquid temperature also reflects in the absence of density and diffusion anomalous regions in the limit of large density of obstacles. Both effects are related to both the entropy increase due to the presence of the obstacles and the disruption of the bonds network.

## ACKNOWLEDGMENTS

We acknowledge the Brazilian agency CAPES (Coordenação de Aperfeiçoamento de Pessoal de Nível Superior) for financial support. C.E.F. acknowledge CNPQ and FAPESP for the financial support under Grants No. 307431/2012-6 and No. 04451-2.

[1] P. C. Hemmer and G. Stell, *Phys. Rev. Lett.* **24**, 1284 (1970).

[2] P. G. Debenedetti, V. S. Raghavan, and S. S. Borick, *J. Phys. Chem.* **95**, 4540 (1991).

- [3] C. H. Cho, S. Singh, and G. W. Robinson, *Phys. Rev. Lett.* **76**, 1651 (1996).
- [4] E. A. Jagla, *Phys. Rev. E* **58**, 1478 (1998).
- [5] P. Camp, *Phys. Rev. E* **68**, 061506 (2003).
- [6] A. B. de Oliveira, P. A. Netz, T. Colla, and M. C. Barbosa, *J. Chem. Phys.* **124**, 084505 (2006).
- [7] Y. D. Fomin, N. V. Gribova, V. N. Ryzhov, S. M. Stishov, and D. Frenkel, *J. Chem. Phys.* **129**, 064512 (2008).
- [8] G. M. Bell and D. A. Lavis, *J. Phys. A* **3**, 568 (1970).
- [9] D. A. Lavis, *J. Phys. C* **6**, 1530 (1973).
- [10] G. Franzese and H. E. Stanley, *J. Phys.: Condens. Matter* **14**, 2201 (2002).
- [11] C. Buzano and M. Pretti, *J. Chem. Phys.* **119**, 3791 (2003).
- [12] V. B. Henriques and M. C. Barbosa, *Phys. Rev. E* **71**, 031504 (2005).
- [13] V. B. Henriques, N. Guissoni, M. A. Barbosa, M. Thielo, and M. C. Barbosa, *Mol. Phys.* **103**, 3001 (2005).
- [14] N. G. Almarza, J. A. Capitan, J. A. Cuesta, and E. Lomba, *J. Chem. Phys.* **131**, 124506 (2009).
- [15] A. L. Balladares, V. B. Henriques, and M. C. Barbosa, *J. Phys.: Condens. Matter* **19**, 116105 (2007).
- [16] M. Szortyka, M. Girardi, V. B. Henriques, and M. C. Barbosa, *J. Chem. Phys.* **130**, 184902 (2009).
- [17] G. S. Kell, *J. Chem. Eng. Data* **20**, 97 (1975).
- [18] C. A. Angell, E. D. Finch, and P. Bach, *J. Chem. Phys.* **65**, 3063 (1976).
- [19] Martin Chaplin, Seventy-two anomalies of water, <http://www.lsbu.ac.uk/water>
- [20] O. Mishima, *Phys. Rev. Lett.* **85**, 334 (2000).
- [21] O. Mishima, *Chem. Phys. Lett.* **422**, 507 (2006).
- [22] P. H. Poole, F. Sciortino, U. Essmann, and H. E. Stanley, *Phys. Rev. E* **48**, 3799 (1993).
- [23] Osamu Mishima, *J. Chem. Phys.* **100**, 5910 (1994).
- [24] P. H. Poole, F. Sciortino, E. Ulrich, and H. E. Stanley, *Nature* **360**, 324 (1992).
- [25] L. Xu, P. Kumar, S. V. Buldyrev, S.-H. Chen, P. Poole, F. Sciortino, and H. E. Stanley, *Proc. Natl. Acad. Sci. USA* **102**, 16558 (2005).
- [26] S.-H. Chen, F. Mallamace, C. Y. Mou, M. Broccio, C. Corsaro, A. Faraone, and L. Liu, *Proc. Natl. Acad. Sci. USA* **103**, 12974 (2006).
- [27] J. R. Bordin, L. B. Krott, and M. C. Barbosa, *J. Phys. Chem. C* **118**, 9497 (2014).
- [28] Leandro B. Krott and Marcia C. Barbosa, *Phys. Rev. E* **89**, 012110 (2014).
- [29] Leandro B. Krott and Marcia C. Barbosa, *J. Chem. Phys.* **138**, 084505 (2013).
- [30] P. Kumar, F. W. Starr, S. V. Buldyrev, and H. E. Stanley, *Phys. Rev. E* **75**, 011202 (2007).
- [31] P. Scheidler, W. Kob, and K. Binder, *Europhys. Lett.* **59**, 701 (2002).
- [32] M. Meyer and H. E. Stanley, *J. Phys. Chem. B* **103**, 9728 (1999).
- [33] N. Giovambattista, P. J. Rossky, and P. G. Debenedetti, *Annu. Rev. Phys. Chem.* **63**, 179 (2012).
- [34] Y. Liu, A. Z. Panagiotopoulos, and P. G. Debenedetti, *J. Chem. Phys.* **132**, 144107 (2010).
- [35] M. C. Gordillo and J. Mart, *J. Phys.: Condens. Matter* **22**, 284111 (2010).
- [36] F. Leoni and G. Franzese, *J. Chem. Phys.* **141**, 174501 (2014).
- [37] J. Bai and X. C. Zeng, *Proc. Natl. Acad. Sci. USA* **109**, 21240 (2012).
- [38] J. R. Bordin, J. S. Andrade, Jr., A. Diehl, and M. C. Barbosa, *J. Chem. Phys.* **140**, 194505 (2014).
- [39] R. Bordin, A. Diehl, and M. C. Barbosa, *J. Phys. Chem. B* **117**, 7047 (2013).
- [40] R. Bordin, A. B. de Oliveira, A. Diehl, and Marcia C. Barbosa, *J. Phys. Chem. B* **137**, 084504 (2012).
- [41] J. R. Bordin, A. Diehl, M. C. Barbosa, and Y. Levin, *Phys. Rev. E* **85**, 031914 (2012).
- [42] D. Corradini, P. Gallo, and M. Rovere, *J. Mol. Liq.* **159**, 18 (2011).
- [43] P. Gallo and M. Rovere, *Phys. Rev. E* **76**, 061202 (2007).
- [44] P. Gallo, M. Rapinesi, and M. Rovere, *J. Chem. Phys.* **117**, 369 (2002).
- [45] P. Gallo, M. Rovere, and S.-H. Chen, *J. Phys. Chem. Lett.* **1**, 729 (2010).
- [46] P. Gallo, M. Rovere, and S.-H. Chen, *J. Phys.: Condens. Matter* **24**, 064109 (2012).
- [47] E. B. Moore, J. T. Allen, and V. Molinero, *J. Phys. Chem. C* **116**, 7507 (2012).
- [48] N. Giovambattista, P. J. Rossky, and P. G. Debenedetti, *Phys. Rev. Lett.* **102**, 050603 (2009).
- [49] P. Kumar, S. V. Buldyrev, F. W. Starr, N. Giovambattista, and H. E. Stanley, *Phys. Rev. E* **72**, 051503 (2005).
- [50] S. R.-V. Castrillon, N. Giovambattista, I. A. Aksay, and P. G. Debenedetti, *J. Chem. Phys. B* **113**, 1438 (2009).
- [51] S. Han, P. Kumar, and H. E. Stanley, *Phys. Rev. E* **77**, 030201 (2008).
- [52] E. G. Strekalova, J. Luo, H. E. Stanley, G. Franzese, and S. V. Buldyrev, *Phys. Rev. Lett* **109**, 105701 (2012).
- [53] E. G. Strekalova, M. G. Mazza, H. E. Stanley, and G. Franzese, *J. Phys.: Condens. Matter* **24**, 064111 (2012).
- [54] E. G. Strekalova, M. G. Mazza, H. E. Stanley, and G. Franzese, *Phys. Rev. Lett.* **106**, 145701 (2011).
- [55] P. A. Bonnaud, B. Coasne, and R. J.-M. Pellenq, *J. Phys.: Condens. Matter* **22**, 284110 (2010).
- [56] O. Pizio, H. Dominguez, L. Pusztai, and S. Sokolowski, *Physica A* **338**, 2278 (2009).
- [57] K. S. Page and P. A. Monson, *Phys. Rev. E* **54**, 6557 (1996).
- [58] S. T. Cui, P. T. Cummings, and H. D. Cochran, *J. Chem. Phys.* **114**, 7189 (2001).
- [59] A. Jabbarzadeh, P. Harrowell, and R. I. Tanner, *J. Chem. Phys.* **125**, 034703 (2006).
- [60] H. Chen, J. K. Johnson, and D. S. Sholl, *J. Phys. Chem. B* **110**, 1971 (2006).
- [61] X. Qin, Q. Yuan, Y. Zhao, S. Xie, and Z. Liu, *Nano Lett.* **11**, 2173 (2011).
- [62] T. Urbic, V. Vlachy, O. Pizio, and K. A. Dill, *J. Mol. Liq.* **112**, 71 (2004).
- [63] A. Kovalenko and F. Hirata, *J. Chem. Phys.* **112**, 10391 (2000).
- [64] D. Frenkel and B. Smit, *Understanding Molecular Simulation: From Algorithms to Applications* (Academic Press, San Diego, 2002).

- [65] N. Metropolis, A. W. Rosenbluth, M. N. Rosenbluth, A. H. Teller, and E. Teller, *J. Chem. Phys.* **21**, 1087 (1953).
- [66] M. Álvarez, D. Levesque, and J.-J. Weis, *Phys. Rev. E* **60**, 5495 (1999).
- [67] J. M. Fish and R. L. C. Vink, *Phys. Rev. Lett.* **105**, 147801 (2010).
- [68] P. A. Netz, F. W. Starr, M. C. Barbosa, and H. E. Stanley, *Physica A* **314**, 470 (2002).